Elucidation of Mechanism for Reducing Porosity in Electric Arc Spraying Through CFD

Ryoji Tamaki[1(✉)] and Masashi Yamakawa[2]

[1] Daihen Co., Ltd., Koyocho-nishi, Higashinada-ku, Kobe, Hyogo, Japan
tamaki@daihen.co.jp
[2] Kyoto Institute of Technology, Matsugasaki, Sakyo-ku, Kyoto, Japan

Abstract. We elucidated the mechanism for reducing the porosity (a means for achieving smaller globules) through Computational Fluid Dynamics while focusing on the flow of compressed air. A simulation study revealed that a spray gun nozzle comprising a flow splitting plate located upstream of the arc point in the nozzle produces compression waves whereby the flow field made in the nozzle differs substantially from that made in a conventional, plate-less nozzle. Observation using a high-speed camera showed that smaller particles of the molten metal (globules) were made due to the plate, which means that the compression waves generated upstream of the arc point affect the formation of globules at the arc point.

Keywords: Electric arc spraying · Compression wave · Compression Expansion

1 Introduction

In a wide range of industries, coating processes called thermal spraying are widely used to repair surfaces of mechanical components, increase hardness, and protect outdoor structural materials such as steel bridges against rust and corrosion (see Table 1). Thermal spray coating is a process in which a melted metallic material is sprayed onto a surface.

Table 1. Purposes of thermal spraying.

Function improvement	Used to improve wear resistance
	Used to give electrical characteristics
Rust and corrosion prevention	Used to prevent outdoor structures from getting rusted and corroded (to protect base materials)
	Used to prevent combustion chambers from getting corroded due to high temperature

Various thermal spray coating methods exist, and they are classified into two types by the method employed to heat coating materials to molten or semi-molten state, as

Y. Shi et al. (Eds.): ICCS 2018, LNCS 10860, pp. 418–428, 2018.
https://doi.org/10.1007/978-3-319-93698-7_32

shown in Fig. 1. Oxy-fuel spraying is subdivided into flame spraying and high-velocity flame spraying. The former utilizes a gas mixture of oxygen and acetylene as a heat source to produce combustion flame together with compressed air to accelerate material globules of micro particles toward the workpiece. High-velocity oxy-fuel (HVOF) coating, another type of flame spraying, utilizes high-pressure oxygen to produce confined combustion at high pressures, and hot gas flame jet that accelerates globules toward the workpiece at extreme velocities.

Electric spraying includes plasma spraying, and electric arc spraying which is the subject of this study. In a plasma-arc gun, an inert gas, typically argon, is charged by electrodes whereby it ionizes to generate hot, high-velocity plasma. Plasma spraying uses this plasma as the heat source. Usually, a water-cooled copper nozzle works as the anode, and the cathode is made of tungsten. For plasma spraying, plasma is generated by electric arc burning within the nozzle of the plasma gun and the arc gas is formed into a plasma jet as it emerges from the nozzle. Powder particles injected into this jet strike the workpiece at high velocity to produce a strongly adherent coating.

Electric arc spraying is a form of thermal spraying where two metal wires which ultimately form the coating are fed independently into the spray gun as shown in Fig. 2. Typical wire materials are aluminum/zinc, copper/copper, and steel/steel for example. These wires are fed into a wire feeding unit and electrically charged via electrodes to generate an arc. The wires placed as they face together produce an electric arc to melt the wires. Compressed air or other gas, passing through a nozzle, atomizes the molten metal and sprays it onto the workpiece (substrate surface).

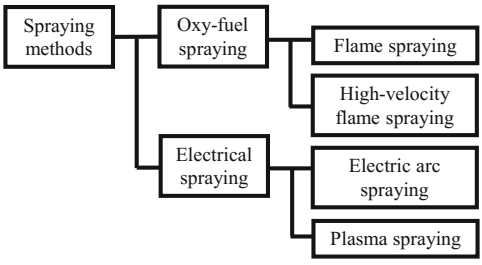

Fig. 1. Spraying methods

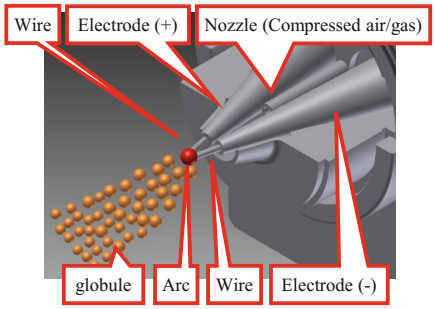

Fig. 2. Arc spraying system

Among the methods described above, the electric arc spraying delivers a high feed rate of spraying in a short period of time and comparatively high spraying quality at low cost. Thanks to these features, it has been commonly used in a wide variety of industries. However, the method suffers from some disadvantages including a large production of fume (atomized particles) worsening the working environment, larger porosity (voids) in the coating compared to other arc spraying methods, and production of oxides during transportation of globules in air leading to entrainment of the oxides in the coating. Especially, the larger porosity is serious as it is detrimental to the coating strength i.e. corrosion resistance. Therefore, we studied how the porosity could be reduced.

Important parameters that affect the formation of coating film in electric arc spraying are arc voltage, wire feed, and compressed air (or gas) flow (i.e. air pressure and nozzle shape). Many of existing studies [1–5] focused on the arc voltage and wire feed only, considering the compressed air flow (air pressure and nozzle shape) less important except the study [6] focused on the compressible flows. This study is to find a mechanism effective for reducing the porosity. To this end, the compressed flow was examined in detail by means of CFD analysis. The computations were carried out in an OpenMP Parallel environment for the unstructured mesh system [7]. As a visualizing aid, a high-speed camera was used for complementing the CFD result.

2 Numerical Simulation

2.1 Computation Method

The methods used for the computation are given in Table 2. As governing equation, following three-dimensional Navier-Stokes equation written in conservation low form is adopted.

$$\frac{\partial \mathrm{U}}{\partial t} + \frac{\partial (\mathrm{E} - \mathrm{E_v})}{\partial x} + \frac{\partial (\mathrm{F} - \mathrm{F_v})}{\partial y} + \frac{\partial (\mathrm{G} - \mathrm{G_v})}{\partial z} = 0 \tag{1}$$

Where, U is a conserved quantity vector. E, F, G and $\mathrm{E_v}$, $\mathrm{F_v}$, $\mathrm{G_v}$ are advection-flux and viscous-flux vectors for x, y, z direction respectively.

For advective term data calculation, Rotated-RHLL method [8] was used. The Rotated-RHLL solver, a method that combines the HLL and Roe solvers, is capable of capturing shock waves, expansion waves and contact surfaces at high resolution while not producing Carbuncle phenomena in which impact wave surfaces tend to be unstable. The representative equations of this method are shown below.

$$\varphi_{RHLL} = \frac{S_R^+ \mathrm{H}_n(\mathrm{U}_L) - S_L^- \mathrm{H}_n(\mathrm{U}_R)}{S_R^+ - S_L^-} - \frac{1}{2} \sum_{k=1}^{4} \left| \widehat{S}_{RHLL}^k \right| \widehat{w}_{n_2}^k \widehat{\mathrm{r}}_{n_2}^k \tag{2}$$

where

$$\left| \widehat{S}_{RHLL}^k \right| = \alpha_2 \left| \widehat{\lambda}_{n_2}^k \right|^* - \frac{1}{S_R^+ - S_L^-} \left[\alpha_2 \left(S_R^+ + S_L^- \right) \widehat{\lambda}_{n_2}^k + \alpha_1 S_R^+ S_L^- \right]. \tag{3}$$

H is combined E, F and G. φ_{RHLL} is combined the Roe flux function and the Rusanov flux function.

For diffusion term calculation and time integration, Alpha-damping scheme [9–11] and Defect Correction method were used respectively, and SST k-ω was used for the turbulence model. The SST k-ω turbulence model behaves well in analyses of flows that involve separation, and therefore can simulate separated flows at higher accuracy than typical turbulence models including k-ω. These calculations used a general purpose thermo-fluid simulation software SC/Tetra [12].

2.2 Computational Model and Boundary Conditions

Figure 3 shows the computational model. The total pressure was given together with temperatures as the inflow condition. A cylindrical open space was provided around the nozzle. Assuming that the entire wall surface of the cylindrical open space served as air outlets, the surface pressure (i.e., atmospheric pressure) was given together with environmental temperature. For detailed condition, refer to Table 3.

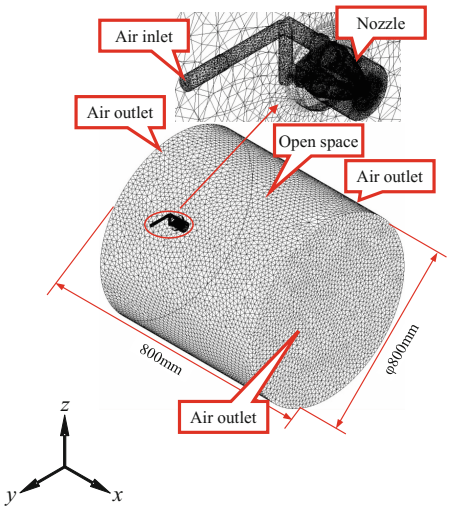

Fig. 3. Computational model

Table 2. Computation Methods

Governing equation	Three-dimensional Navier-Stokes equation
Advective term	Rotated-RHLL method [8]
Diffusion term	Alpha-damping scheme [9–11]
Time integration	Defect correction method
Steady/Unsteady flow	Steady
Turbulence model	SST k-ω

Table 3. Boundary conditions

Inflow condition	Total pressure regulation (0.4 MPa at 39 °C)
Outflow condition	Surface pressure regulation (0.0 MPa at 29 °C)
Wall surface	Stationary wall

As shown in Fig. 4, computations were performed for a total of four different types of nozzle, which included one nozzle of 6 mm in aperture diameter (normal nozzle) and three nozzle that sprayed no jet flow directly to the arc point by mounting a plate on the upstream side from the arc point (i.e., three types of splitter nozzle of 6 mm in aperture nozzle). The plate of 1 mm in width and 6 mm in length was located in the nozzle at L = 0.5 mm, 1.0 mm and 2.0 mm in the distance from the nozzle tip (see Table 4).

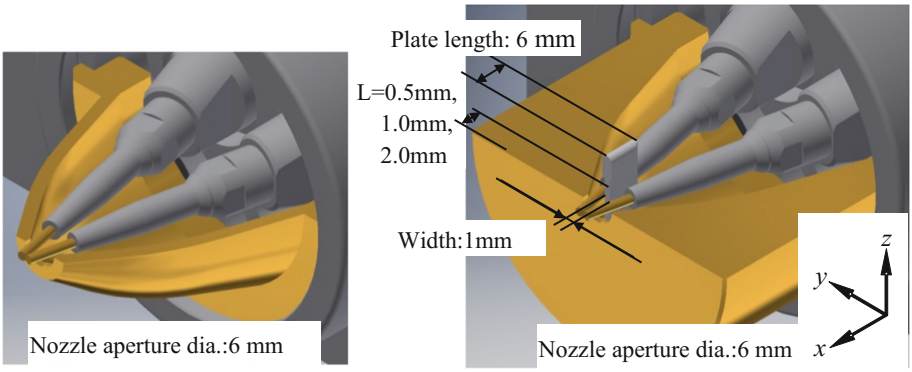

Fig. 4. Nozzle

Table 4. Splitter nozzles

Name	Distance between nozzle tip and plate	Plate size
Splitter nozzle 1	0.5 mm	1 mm in width × 6 mm in length
Splitter nozzle 2	1.0 mm	
Splitter nozzle 3	2.0 mm	

3 Simulation Result

Figure 5 shows the Mach numbers measured in the *xy* and *yz* planes for the normal nozzle. The distance from the nozzle tip to the workpiece is normally 100 to 200 mm. Seeing the enlarged view of the *xy* plane, it was found that the jet flow compresses after leaving the nozzle. Then it undergoes a cycle of expansion and compression while reducing its width. In the *yz* plane, the jet flow first compresses on the top and bottom surface of the wire at the nozzle aperture and then repeats a cycle of expansion and compression while reducing its width. Seeing the enlarged view to look deep into the jet flow behavior in and around the nozzle tip, larger Mach numbers are measured at closer to the nozzle tip with a Mach number of higher than 2 measured at the arc point. However, in reality, the behavior in this region cannot be simulated accurately since plasma can occur near the arc point due to the heat produced by arc discharge between the wires.

As mentioned above, for the normal nozzle, larger Mach numbers are measured at closer to the nozzle tip; and then the jet flow undergoes a cycle of expansion and compression while reducing its width. The expansion and compression process pulverizes the molten metal into micro globules. Of these, those flowing at high speed at around the center of the nozzle will collide with the workpiece leading to the formation of a film of coating.

For a configuration with a plate located 0.5 mm upstream of the nozzle aperture (splitter nozzle 1), Mach number measurements in the *xy* and *yz* planes are shown in

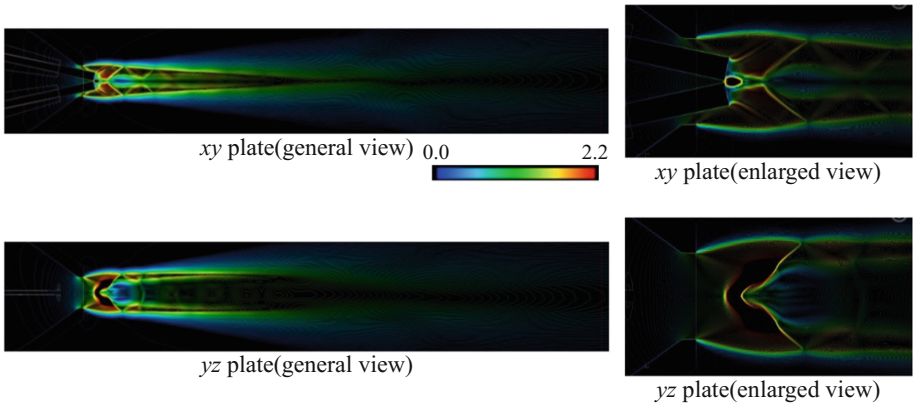

Fig. 5. Mach number contour for the normal nozzle

Fig. 6. In the *xy* plane, compression waves are generated on both sides of the plate. The flow pattern after the nozzle is different from that of the normal nozzle. This is attributed to the plate that changes the flow field in the nozzle.

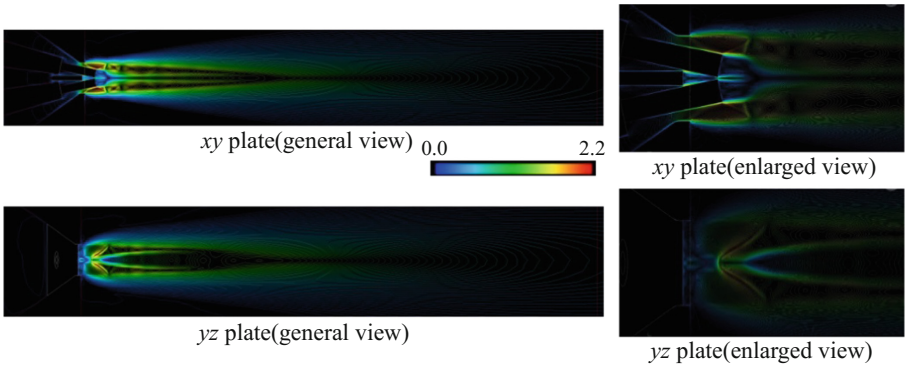

Fig. 6. Mach number contour for the splitter nozzle 1

The configuration with a plate located 1.0 mm upstream of the nozzle aperture (splitter nozzle 2) produces larger compression waves than the configuration with a plate located 0.5 mm upstream of the nozzle aperture. Since this calculation assumes a constant inflow pressure of 0.4 MPa, the plate located closer to the nozzle aperture produces a larger pressure drop at the nozzle aperture. This is probably the reason for the smaller compression waves produced by the plate located 0.5 mm upstream of the nozzle aperture compared to the configuration with the plate located 1.0 mm upstream.

The configuration with a plate located 2.0 mm upstream of the nozzle aperture (splitter nozzle 3) also causes compression waves to be generated on both sides of the plate. However, these compression waves are smaller than those generated by other

configurations with a plate located 1.0 mm or 0.5 mm upstream of the nozzle aperture. This is probably because the larger distance between the plate and nozzle aperture may lead to a smaller compression (reduction) of the flow sectional area (Fig. 7).

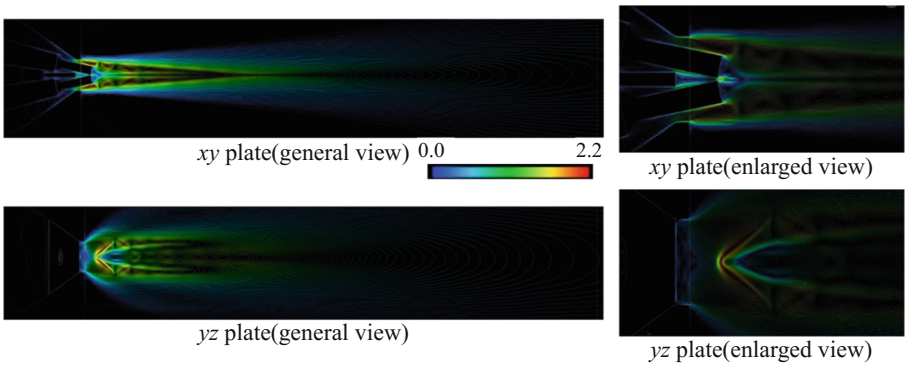

Fig. 7. Mach number contour for the splitter nozzle 2

As mentioned above, with a plate located in the nozzle, compression waves occur in the nozzle, which changes the flow field greatly from that can occur in a conventional, plate-less nozzle (Fig. 8).

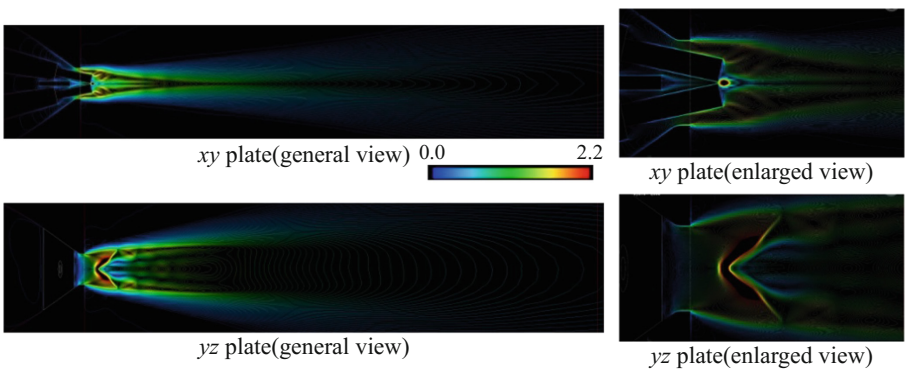

Fig. 8. Mach number contour for the splitter nozzle 3

4 Experimental Method

4.1 Experimental System

To visualize the results of the simulation i.e. the effect of the change in flow field on arc spraying, an experiment was performed using a high-speed camera. The experiment used the equipment shown in Fig. 9, φ1.6 iron-based solid wires (ISO common id:

G49A2UM15) showing a relatively better feedability, thermal spray gun ASTS-2501 manufactured by Daihen, the normal nozzle and splitter nozzle 2 as mentioned above, and power supply unit AS-400 manufactured by Daihen with a reactor inserted between the power unit and the gun. The reactor complemented the power unit AS-400 to supply the power required for melting the iron wires.

A high-speed camera HX-3 of NAC make was used with a shutter speed of $1/10^9$ s and 30000 frames per second. Details of thermal spraying conditions are as shown in Table 5.

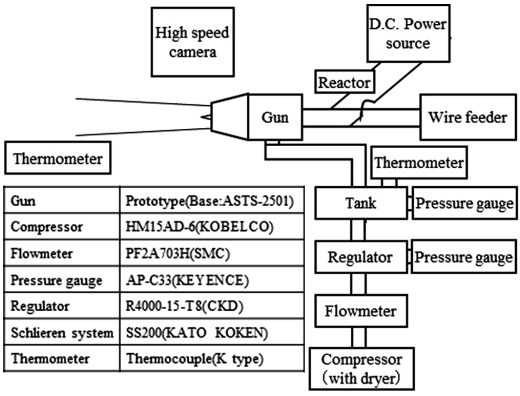

Fig. 9. Experiment schematic

Table 5. Thermal spraying conditions

Tank pressure	0.4 MPa
Wire feeding speed	7.0 m/min
Average arc voltage	26.5 V
Type of wire	φ1.6 iron-based solid wires

5 Result of Experiment

Figure 10 shows a visualization (8 frames, 1/30000 s/frame) of the region around the arc point for the normal nozzle. In the images ([1] through [8]), areas in white represent arcs. They are shown in white because backlighting to extinguish arc lights is not used. These pictures show that the wire is melted by arc heat, and elongated and torn by the flow of compressed air to small globules (areas circled in red in Fig. 10).

Figure 11 shows the same visualization for the splitter nozzle 2. As is the case with the normal nozzle, areas in white represent arcs. Compared to the case with the normal nozzle, the globules made by tearing the arc-heated molten wire are smaller (areas circled in blue in Fig. 11). The simulation mentioned above indicated that the splitter nozzle causes compression waves to be generated on the plate located upstream of the arc point. These compression waves affect the production of globules (pulverization of molten metal) at the arc point.

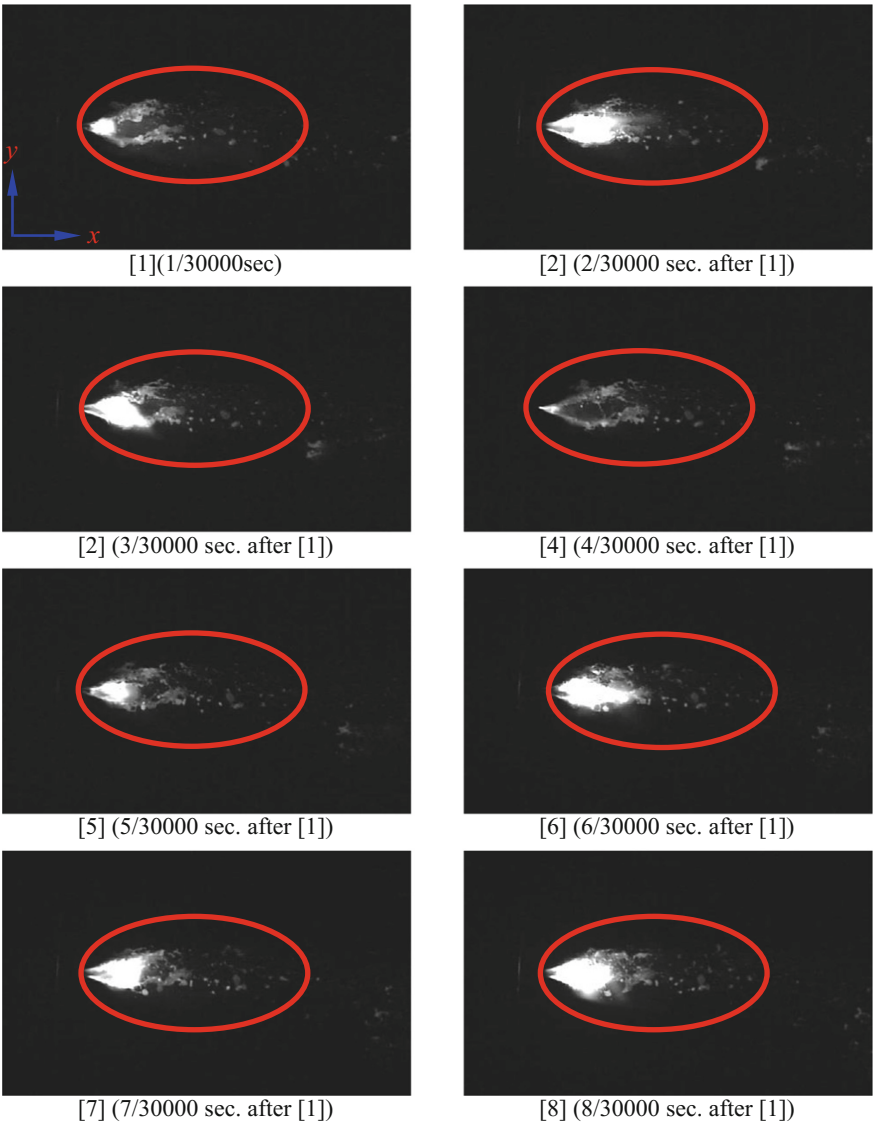

Fig. 10. Visualization for normal nozzle (around the nozzle tip) (Color figure online)

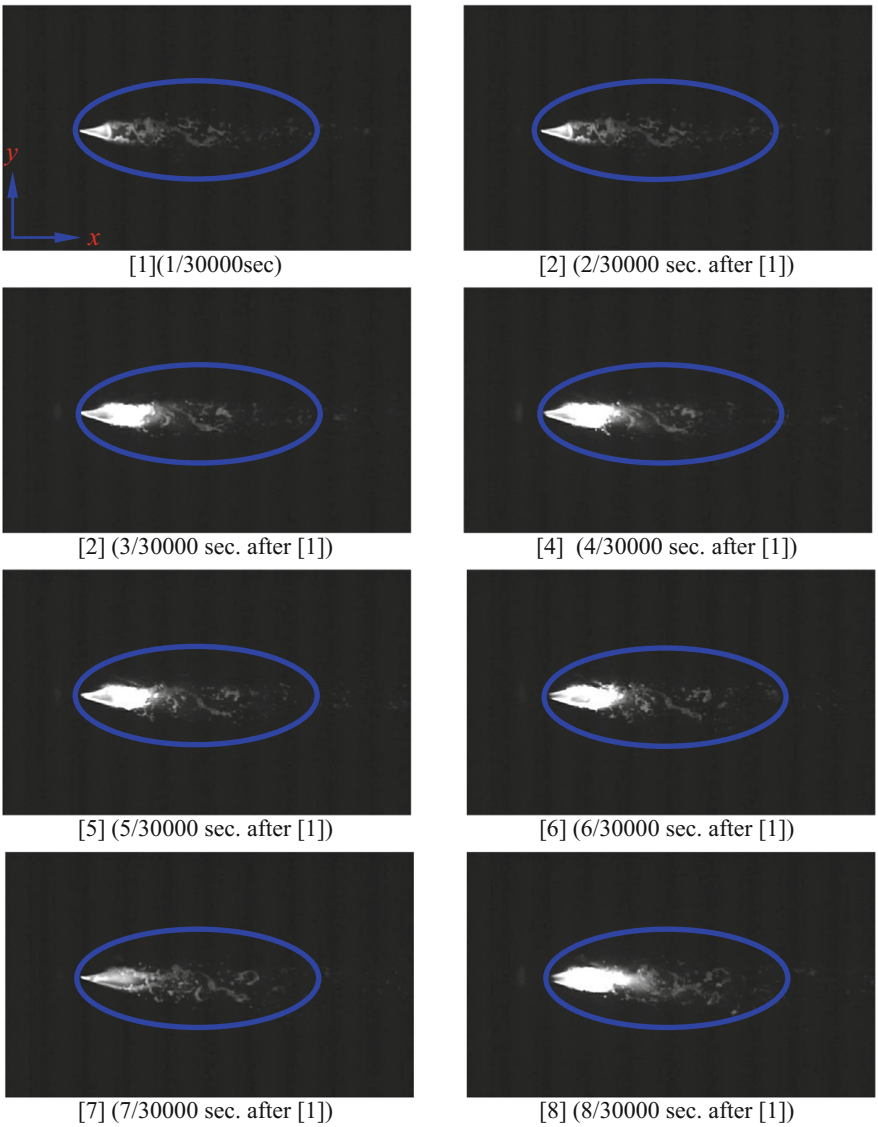

Fig. 11. Visualization for splitter nozzle 2 (around the nozzle tip) (Color figure online)

6 Conclusions

In this study, we aimed to elucidate the properties of a jet flow spurting from the arc spray gun nozzle, and the data presented here supports the following:

1. CFD analyses indicated that, in the normal nozzle, the flow from the nozzle aperture undergoes a cycle of expansion and compression leading to damping. This

expansion and compression process can be considered a cause of molten metal pulverization.
2. CFD analysis indicated that the splitter nozzle, that is, a nozzle with a plate located upstream of the arc point, produces compression waves on the plate, so that the flow field is greatly different from that observed in the normal nozzle.
3. Visualization using a high-speed camera revealed that the splitter nozzle produces molten metal globules of smaller size, which means that the compression waves generated before the arc point affect the process of molten metal pulverization into micro globules.

References

1. Watanabe, T., Usui, M.: Effect of atomizing gas on oxidation of droplets in wire arc spraying. J. Jpn. Inst. Met. **63**, 98–102 (1999)
2. Kawase, R., Kureishi, M., Minehisa, S.: Relation between arc spraying condition and adhesion strength of sprayed coatings. J. JWS 17–22 (1983)
3. Kawase, R., Kureishi, M., Maehara, K.: Arc phenomenon and wire fusion in arc spraying. J. JWS, 82–87 (1984)
4. Kawase, R., Kureishi, M.: Fused metal temperature in arc spraying. J. JWS, 52–58 (1984)
5. Kawase, R., Kureishi, M.: Relation between adhesion strength of sprayed coating and fused metal temperature. J. JWS, 21–260 (1985)
6. Tamaki, R., Yamakawa, M.: Study on the nozzle jet in arc spraying. Appl. Math. Mech. **37** (12), 1394–1402 (2016)
7. Yamakawa, M., Kita, Y., Matsuno, K.: Domain decomposition method for unstructured meshes in an OpenMP computing environment. Comput. Fluids **45**, 168–171 (2011)
8. Nishikawa, H., Kitamura, K.: Very simple, carbuncle-free, boundary-layer-resolving, rotated-hybrid Riemann solvers. J. Comput. Phys. **227**, 2560–2581 (2008)
9. Nishikawa, H.: Beyond interface gradient: a general principle for constructing diffusion schemes. In: AIAA Paper, pp. 2010–5093 (2010)
10. Nishikawa, H.: Robust and accurate viscous discretization via upwind scheme-I: basic principle. Comput. Fluids **49**, 62–86 (2011)
11. Nishikawa, H.: Two ways to extend diffusion schemes to Navier-Stokes schemes: gradient formula or upwind flux. In: AIAA Paper, pp. 2011–3044 (2011)
12. http://www.cradle-cfd.com/